


## Spin-density wave state in simple hexagonal graphite

K. S. Mosoyan,<sup>1</sup> A. V. Rozhkov,<sup>1,2</sup> A. O. Sboychakov,<sup>2</sup> and A. L. Rakhmanov<sup>1,2,3</sup>

<sup>1</sup>*Moscow Institute for Physics and Technology (State University), Moscow region, 141700 Russia*

<sup>2</sup>*Institute for Theoretical and Applied Electrodynamics, Russian Academy of Sciences, Moscow, 125412 Russia*

<sup>3</sup>*Dukhov Research Institute of Automatics, Moscow, 127055 Russia*

 (Received 12 October 2017; revised manuscript received 28 December 2017; published 14 February 2018)

Simple hexagonal graphite, also known as AA graphite, is a metastable configuration of graphite. Using tight-binding approximation, it is easy to show that AA graphite is a metal with well-defined Fermi surface. The Fermi surface consists of two sheets, each shaped like a rugby ball. One sheet corresponds to electron states, another corresponds to hole states. The Fermi surface demonstrates good nesting: a suitable translation in the reciprocal space superposes one sheet onto another. In the presence of the electron-electron repulsion, a nested Fermi surface is unstable with respect to spin-density-wave ordering. This instability is studied using the mean-field theory at zero temperature, and the spin-density-wave order parameter is evaluated.

DOI: [10.1103/PhysRevB.97.075131](https://doi.org/10.1103/PhysRevB.97.075131)

### I. INTRODUCTION

Since recent isolation of the graphene layer [1], the interest to layered carbon systems was reignited. It has been known for some time already that such systems are very diverse, and demonstrate interesting many-body electron properties. For example, graphite in magnetic field undergoes [2] a transition into a field-induced charge-density-wave (CDW) state. After intercalation, graphite may become a superconductor. For example [3], the critical temperature for graphite intercalated with Ca equals to  $T_c = 11.5$  K, as for Yb-intercalated graphite, it is characterized by  $T_c = 6.5$  K.

In this paper, a purely carbon system, simple hexagonal graphite [also known as AA graphite (AA-G)] is discussed. A fragment of simple hexagonal lattice is shown in Fig. 1. It is believed [4] that the simple hexagonal lattice has higher energy than the hexagonal (also referred to as ABA) and rhombohedral (ABC) lattices. In other words, among the three possible highly symmetric layered structures of carbon, the simple hexagonal lattice is the least stable. This implies that experimental realization of the AA-G is bound to run into difficulties: AA lattice will try to relax into either ABA or ABC structures to reduce the chemical energy. Yet, samples of AA-G (as well as bilayer and multilayer AA graphene, which are similar to the AA-G) were synthesized by several groups [5–8]. These experimental advances make the studies of electron properties of the AA-G a timely theoretical task.

From the band theory standpoint, the AA-G is a metal with a well-defined Fermi surface [4,9,10]. The Fermi surface consists of two sheets, or two components. One component corresponds to electron states, the other component corresponds to hole states. Both sheets have shapes of rugby balls. The sheet shapes are almost identical, and suitable translation superposes them. The latter property of the Fermi surface is called nesting.

A Fermi surface with the nesting is unstable with respect to the spin-density-wave (SDW) order. The instability is driven by electron-electron repulsion. The main purpose of this paper is to discuss the SDW instability of the AA-G electronic liquid at zero temperature. Using tight-binding approximation, we

will evaluate the Fermi surface structure of the AA-G, and demonstrate that the nesting of the Fermi surface is indeed present. After that, the SDW zero-temperature state will be studied with the help of mean-field approximation.

The paper is organized as follows. In Sec. II we formulate the tight-binding description of the AA-G. The zero-temperature mean-field calculations are performed in Sec. III. Finally, Sec. IV presents both the discussion and the conclusions of the study. Technically involved details are relegated to the Appendices.

### II. TIGHT-BINDING MODEL OF THE AA GRAPHITE

#### A. Geometry and tight-binding description of graphene

Tight-binding model of the AA-G is a straightforward generalization of the tight-binding model of graphene. The latter is mostly determined by the geometrical properties of the honeycomb lattice of graphene (for more details, one can consult a review on graphene, for example, Ref. [11]). The graphene has hexagonal lattice consisting of two triangular sublattices *A* and *B* (see Fig. 1). Thus, the elementary unit cell of graphene contains two atoms. The elementary translation vectors may be chosen as follows:

$$\mathbf{a}_1 = \frac{a}{2}(3, -\sqrt{3}), \quad \mathbf{a}_2 = \frac{a}{2}(3, \sqrt{3}), \quad (1)$$

where  $a \approx 1.42$  Å is the distance between the nearest-neighbor carbon atoms. The reciprocal lattice vectors are

$$\mathbf{b}_1 = \frac{2\pi}{3a}(1, -\sqrt{3}), \quad \mathbf{b}_2 = \frac{2\pi}{3a}(1, \sqrt{3}). \quad (2)$$

The Dirac cones of the graphene are located in the corners of the hexagonal Brillouin zone. Without loss of generality, we can assume that these cones are centered at points

$$\mathbf{K} = \left( \frac{2\pi}{3a}, \frac{2\pi}{3\sqrt{3}a} \right), \quad \mathbf{K}' = \left( \frac{2\pi}{3a}, -\frac{2\pi}{3\sqrt{3}a} \right). \quad (3)$$

For the single layer (thus, abbreviation “sl”) of graphene, the simplest tight-binding Hamiltonian for  $\pi$  bonds of carbon

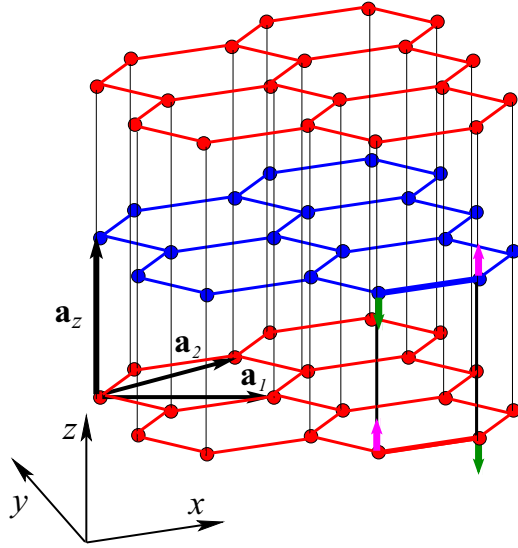


FIG. 1. Simple hexagonal lattice of AA graphite. It consists of layers of graphene stacked upon each other. Lattice vectors are  $\mathbf{a}_1$ ,  $\mathbf{a}_2$ , and  $\mathbf{a}_z$ . The distance between neighboring atoms inside the layer is  $a = 1.42 \text{ \AA}$ , while the distance between the layers is  $c \equiv |\mathbf{a}_z| \approx 3.3 \text{ \AA}$  according to Ref. [4] and  $c \approx 3.4 \text{ \AA}$  according to Ref. [5]. Elementary unit cell of the lattice of AA graphite consists of two atoms corresponding to two nonequivalent sublattices of the graphene layer. The SDW ordering doubles the lattice period in the  $z$  direction, making spins configurations in neighboring graphene layers different from each other. As a result, the magnetic unit cell contains four atoms. Short thick arrows show the spin configuration inside this unit cell.

atoms equals

$$H^{\text{sl}} = -t \sum_{\langle \mathbf{n}\mathbf{m} \rangle \sigma} (d_{\mathbf{n}A\sigma}^\dagger d_{\mathbf{m}B\sigma} + \text{H.c.}). \quad (4)$$

Here,  $d_{\mathbf{n}\alpha\sigma}^\dagger$  and  $d_{\mathbf{n}\alpha\sigma}$  are the creation and annihilation operators of the electron with spin projection  $\sigma$ , located at the unit cell  $\mathbf{n} = (n, m)$  ( $n$  and  $m$  are integers) in the sublattice  $\alpha = A, B$ . The summation in Eq. (4) is performed over nearest-neighbor sites, and  $t \approx 2.7 \text{ eV}$  is the nearest-neighbor hopping integral. We introduce the Fourier-transformed electronic operators  $d_{\mathbf{k}\alpha\sigma} = \sum_{\mathbf{n}} e^{i\mathbf{k}\mathbf{r}_{\mathbf{n}}^\alpha} d_{\mathbf{n}\alpha\sigma} / \sqrt{\mathcal{N}}$ , where  $\mathbf{r}_{\mathbf{n}}^\alpha$  is the position of a carbon atom in the  $\mathbf{n}$ th unit cell for sublattice  $\alpha$ , while  $\mathcal{N}$  is the number of unit cells in the sample. We also define the (pseudo)spinor

$$\psi_{\mathbf{k}\sigma} = \begin{pmatrix} d_{\mathbf{k}A\sigma} \\ d_{\mathbf{k}B\sigma} \end{pmatrix}. \quad (5)$$

The Hamiltonian (4) can be rewritten as

$$H^{\text{sl}} = \sum_{\mathbf{k}\sigma} \psi_{\mathbf{k}\sigma}^\dagger \hat{H}_{\mathbf{k}}^{\text{sl}} \psi_{\mathbf{k}\sigma}, \quad (6)$$

where  $2 \times 2$  matrix  $\hat{H}_{\mathbf{k}}^{\text{sl}}$  is

$$\hat{H}_{\mathbf{k}}^{\text{sl}} = -t \begin{pmatrix} 0 & f(\mathbf{k}) \\ f^*(\mathbf{k}) & 0 \end{pmatrix}. \quad (7)$$

In this expression, function  $f$  is equal to

$$f(\mathbf{k}) = e^{-iak_x} \left[ 1 + 2e^{3iak_x/2} \cos\left(\frac{\sqrt{3}}{2}ak_y\right) \right]. \quad (8)$$

For a given value of quasimomentum  $\mathbf{k}$ , the eigenvalues of Eq. (6) are equal to  $\varepsilon_{\mathbf{k}}^{(1,2)} = \pm t|f(\mathbf{k})|$ . Near the Brillouin zone corners, function  $f(\mathbf{k})$  can be expanded as

$$f(\mathbf{K} + \mathbf{q}) \approx \frac{3a}{2} e^{-\frac{2\pi i}{3}} (q_y - iq_x), \quad (9)$$

$$f(\mathbf{K}' + \mathbf{q}) \approx \frac{3a}{2} e^{-\frac{2\pi i}{3}} (-q_y - iq_x). \quad (10)$$

If we substitute Eqs. (9) and (10) into Hamiltonian (6), the latter becomes equivalent to two two-dimensional (2D) Dirac-Weyl Hamiltonians of massless relativistic fermions. Their dispersion is

$$\varepsilon_{\mathbf{q}}^{(1,2)} = \pm v_F |\mathbf{q}|. \quad (11)$$

Here, the Fermi velocity  $v_F = 3at/2$  plays the role of speed of light.

## B. Tight-binding description of the AA graphite

Hamiltonian (6) can be easily modified to describe AA graphite. The generalized Hamiltonian should account for a macroscopic number of stacked graphene layers coupled by single-electron hopping. Electrons with different spins are decoupled from each other. Consequently, we can write

$$H^{\text{AA}} = \sum_{\sigma} H_{\sigma}^{\text{AA}}, \quad (12)$$

where

$$H_{\sigma}^{\text{AA}} = -t \sum_{\langle \mathbf{n}\mathbf{m} \rangle i} (d_{\mathbf{n}iA\sigma}^\dagger d_{\mathbf{m}iB\sigma} + \text{H.c.}) - t_0 \sum_{\mathbf{n}i\alpha} (d_{\mathbf{n}i+1\alpha\sigma}^\dagger d_{\mathbf{n}i\alpha\sigma} + \text{H.c.}). \quad (13)$$

In this expression, integer  $i$  enumerates the layers. The first sum describes the in-layer electron hopping, while the second sum corresponds to the nearest-neighbor interlayer hopping. The interlayer hopping amplitude  $t_0$  is about 0.3–0.4 eV.

Elementary unit cell of the AA-G contains two atoms and is characterized by vectors  $\mathbf{a}_1$ ,  $\mathbf{a}_2$ , and  $\mathbf{a}_z = c \mathbf{e}_z$ , where  $\mathbf{e}_z$  is the unit vector along the  $z$  axis perpendicular to the layers, while  $c \approx 3.3 \text{ \AA}$  is the interlayer distance. Reciprocal unit cell of the AA-G is characterized by vectors  $\mathbf{b}_1$ ,  $\mathbf{b}_2$ , and  $\mathbf{b}_z = 2\pi \mathbf{e}_z/c$ . We introduce Fourier-transformed operators

$$d_{\mathbf{k}\alpha\sigma} = \frac{1}{\sqrt{\mathcal{N}}} \sum_{\mathbf{n}j} e^{i\mathbf{k}\mathbf{r}_{\mathbf{n}j}^\alpha} d_{\mathbf{n}j\alpha\sigma}. \quad (14)$$

Here, vectors  $\mathbf{r}_{\mathbf{n}j}^\alpha = \mathbf{r}_{\mathbf{n}}^\alpha + j\mathbf{a}_z$  describe positions of sites in the AA graphite,  $\mathcal{N}$  is the number of elementary unit cells in the three-dimensional (3D) sample of graphite, and  $\mathbf{k} = (k_x, k_y, k_z)$  now is a 3D momentum. Its 2D projection,  $\mathbf{k}_{\parallel} = (k_x, k_y)$ , is confined to the usual hexagonal Brillouin zone of the single-layer graphene, while  $k_z$  lies in the region  $0 < k_z < 2\pi/c$ . The Brillouin zone of the AA-G has a shape of right hexagonal prism with height  $2\pi/c$  (see Fig. 2).

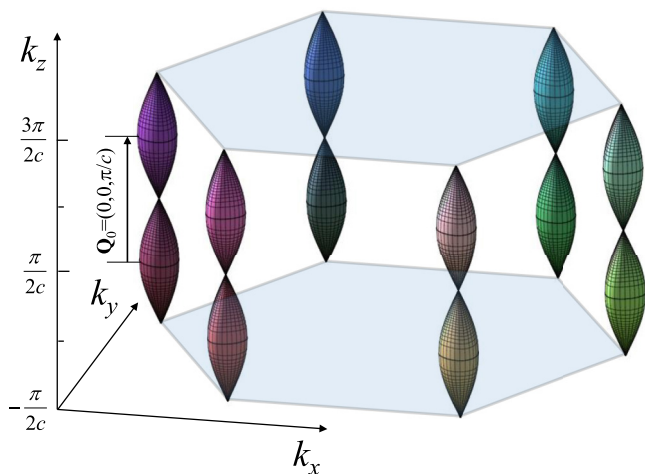


FIG. 2. Fermi surface of the AA-G inside the first Brillouin zone calculated for  $t = 2.7$  eV and  $t_0 = 0.4$  eV. The Brillouin zone is shifted by  $-\pi/(2c)$  along the  $z$  axis for clarity. The Fermi surface emerges near each corner of the Brillouin zone. The Fermi surface consists of two sheets with a shape of a rugby ball. The lower sheet is electronlike, while the upper one is the holelike. Two sheets coincide upon the translation by the nesting vector  $\mathbf{Q}_0 = (0, 0, \pi/c)$ .

In terms of spinor (5) (where now  $\mathbf{k}$  is the 3D vector), Hamiltonian (13) takes the form

$$H_{\sigma}^{\text{AA}} = - \sum_{\mathbf{k}} \psi_{\mathbf{k}\sigma}^{\dagger} \begin{pmatrix} 2t_0 \cos(k_z c) & t f(\mathbf{k}_{\parallel}) \\ t f^*(\mathbf{k}_{\parallel}) & 2t_0 \cos(k_z c) \end{pmatrix} \psi_{\mathbf{k}\sigma}. \quad (15)$$

This Hamiltonian can be easily diagonalized. The corresponding bands are

$$\begin{aligned} \varepsilon_{\mathbf{k}}^{(1)} &= -2t_0 \cos(k_z c) - t |f(\mathbf{k}_{\parallel})|, \\ \varepsilon_{\mathbf{k}}^{(2)} &= -2t_0 \cos(k_z c) + t |f(\mathbf{k}_{\parallel})|. \end{aligned} \quad (16)$$

In a generic situation, the Fermi surface of the AA-G consists of two sheets defined by equations  $\varepsilon^{(1,2)} = \mu$ , where  $\mu$  is the chemical potential. In this paper, we consider the undoped compound only. As we will show below, this corresponds to the case  $\mu = 0$ . For such a value of  $\mu$  the Fermi surface sheets are given by the relations

$$\varepsilon_{\mathbf{k}}^{(1)} = 0 \Rightarrow 2t_0 \cos(k_z c) = -t |f(\mathbf{k}_{\parallel})|, \quad (17)$$

$$\varepsilon_{\mathbf{k}}^{(2)} = 0 \Rightarrow 2t_0 \cos(k_z c) = t |f(\mathbf{k}_{\parallel})|. \quad (18)$$

The AA-G Fermi surface is shown in Fig. 2. The sheet corresponding to the band  $\varepsilon_{\mathbf{k}}^{(1)}$  is the hole sheet because the component of the velocity vector  $\mathbf{v}_{\mathbf{k}}^{(1)} = \partial \varepsilon_{\mathbf{k}}^{(1)} / \partial \mathbf{k}$  normal to the sheet is negative for all momenta on this sheet. Similarly, one can prove that the sheet corresponding to the band  $\varepsilon_{\mathbf{k}}^{(2)}$  is electronlike. The states inside the electron (hole) sheet are filled (empty). Since the sheets have identical volumes, the total number of electrons in the system per atom is equal to unity. Thus, the case  $\mu = 0$ , indeed, corresponds to the undoped AA-G. The Fermi surface of the AA-G has been studied in several publications [4,9,10]. The results of these studies are similar to those shown in Fig. 2.

The surfaces specified by Eqs. (17) and (18) can be superposed by a parallel translation along the  $z$  axis. Indeed, after transformation  $k_z \rightarrow k_z + \pi/c$ , Eq. (17) becomes Eq. (18), and vice versa. When a hole Fermi surface sheet may be superposed with an electron sheet by a suitable translation in momentum space, one refers to such a Fermi surface as nested. The translation vector superposing the sheets is called a nesting vector. In our case, the nesting vector is

$$\mathbf{Q}_0 = \left(0, 0, \frac{\pi}{c}\right). \quad (19)$$

The bands  $\varepsilon_{\mathbf{k}}^{(1)}$  and  $\varepsilon_{\mathbf{k}}^{(2)}$  satisfy the relation  $\varepsilon_{\mathbf{k}+\mathbf{Q}_0}^{(1)} = -\varepsilon_{\mathbf{k}}^{(2)}$ . A Fermi surface with nesting becomes unstable in the presence of arbitrary weak electron-electron repulsion. Vector  $\mathbf{Q}_0$  characterizes the spatial oscillations of the most unstable mode. The instability will be discussed in the next section.

### III. SPIN-DENSITY WAVE IN THE AA GRAPHITE

The instability of the electron liquid with a nested Fermi surface is a well-known feature. In the majority of papers studying the systems with Fermi surface nesting, it is accepted that the electron-electron interaction stabilizes the spin-density-wave ground state. Such a picture is used, for example, to describe antiferromagnetism in chromium and its alloys [12,13], superconducting iron pnictides [14–16], and AA-stacked bilayer graphene [17–19]. Minimal model with electron interaction is the Hubbard model. It accounts for onsite electron-electron interaction only. In this paper, we will study the AA-G version of the Hubbard model in the framework of the mean-field approximation. The Hamiltonian of this model is  $H = H^{\text{AA}} + H_{\text{int}}$ , where  $H^{\text{AA}}$  is given by Eq. (12), and

$$H_{\text{int}} = U \sum_{\mathbf{n}i\alpha} \left( n_{\mathbf{n}i\alpha\uparrow} - \frac{1}{2} \right) \left( n_{\mathbf{n}i\alpha\downarrow} - \frac{1}{2} \right). \quad (20)$$

Parameter  $U > 0$  characterizes onsite electron-electron repulsion, and operator  $n_{\mathbf{n}i\alpha\sigma} = d_{\mathbf{n}i\alpha\sigma}^{\dagger} d_{\mathbf{n}i\alpha\sigma}$ .

In the SDW state, each site acquires a nonzero magnetic moment. We assume here that all spins are directed parallel or antiparallel to the  $z$  axis. Thus, the nonzero spin projections are  $S_{\mathbf{n}i\alpha}^z = (\langle n_{\mathbf{n}i\alpha\uparrow} \rangle - \langle n_{\mathbf{n}i\alpha\downarrow} \rangle) / 2$ . We assume also that the total charge in each site remains constant, that is,  $\langle n_{\mathbf{n}i\alpha\uparrow} \rangle + \langle n_{\mathbf{n}i\alpha\downarrow} \rangle = 1$ . The nesting vector  $\mathbf{Q}_0$  determines the form of the spin-density wave in real space. Specifically, one can write for the SDW state under study the following equality:

$$S_{\mathbf{n}j\alpha}^z = e^{i\mathbf{Q}_0 \cdot \mathbf{r}_{\mathbf{n}j}^{\alpha}} S_{\alpha}. \quad (21)$$

Substituting expression (19) for  $\mathbf{Q}_0$  into Eq. (21), one derives

$$S_{\mathbf{n}j\alpha}^z = (-1)^j S_{\alpha}. \quad (22)$$

This shows that spin arrangements in odd and even layers are different from each other: spin polarizations at two sites separated by vector  $\mathbf{a}_z$  are antiparallel. Yet, Eq. (22) does not specify  $S_{\alpha}$ . Precise structure of  $S_{\alpha}$  has physically relevant consequences. For example, the case  $S_A = S_B$  corresponds to the antiferromagnetically ordered ferromagnetic layers, while in the case  $S_A = -S_B$  we obtain the so-called G-type antiferromagnetism, where both in-plane and out-of-plane neighboring spins are antiparallel. One can prove that for the

case  $S_A = S_B$ , the gap at the Fermi level does not arise and this state is unstable. At the same time, the SDW state with  $S_A = -S_B$  does open the gap at the Fermi level for arbitrary small  $U$ , and corresponds to the mean-field ground state of the model (20). Spin configuration for this SDW order is shown in Fig. 1.

To describe such an ordered state, we introduce the SDW order parameter

$$\Delta_{i\alpha} = \frac{U}{2}(\bar{n}_{i\alpha\uparrow} - \bar{n}_{i\alpha\downarrow}). \quad (23)$$

Here,  $\bar{n}_{i\alpha\sigma} = \langle n_{ni\alpha\sigma} \rangle$ . The order parameter satisfies the conditions

$$\Delta_{i\alpha} = (-1)^i \Delta_\alpha, \quad \Delta_A = -\Delta_B \equiv \Delta. \quad (24)$$

In mean-field approximation, we decompose the density operator in Eq. (20) as follows:  $n_{ni\alpha\sigma} = \bar{n}_{i\alpha\sigma} + \delta n_{ni\alpha\sigma}$ , where operators  $\delta n_{ni\alpha\sigma} = n_{ni\alpha\sigma} - \bar{n}_{i\alpha\sigma}$  describe fluctuations near the average density  $\bar{n}_{i\alpha\sigma}$ . Mean-field interaction Hamiltonian is obtained by neglecting the terms quadratic in  $\delta n_{ni\alpha\sigma}$ . As a result, we derive

$$H_{\text{int}}^{\text{MF}} = \sum_{ni\alpha} \left[ -\Delta_{i\alpha}(n_{ni\alpha\uparrow} - n_{ni\alpha\downarrow}) + \frac{\Delta_{i\alpha}^2}{U} \right]. \quad (25)$$

The considered SDW state doubles the lattice period in the  $z$  direction, while preserving the translation invariance along the layers. Consequently, the elementary cell in the ordered phase contains four sites: two sites in one layer and two sites in an adjacent layer. Due to the doubling of the elementary cell, the Brillouin zone shrinks in the  $k_z$  direction: now, projection  $k_z$  varies from 0 to  $\pi/c$ . For further analysis, it is convenient to introduce the following 4-component spinor:

$$\Psi_{\mathbf{k}\sigma} = \sqrt{\frac{2}{\mathcal{N}}} \sum_{\mathbf{n}j} e^{i\mathbf{k}\mathbf{r}_{\mathbf{n}2j}^\sigma} \begin{pmatrix} d_{\mathbf{n}2jA\sigma} \\ d_{\mathbf{n}2jB\sigma} \\ d_{\mathbf{n}2j+1A\sigma} \\ d_{\mathbf{n}2j+1B\sigma} \end{pmatrix}. \quad (26)$$

In terms of this spinor, the total mean-field Hamiltonian can be written as

$$H^{\text{MF}} = 2\mathcal{N} \frac{\Delta^2}{U} + \sum_{\mathbf{k}\sigma}' \Psi_{\mathbf{k}\sigma}^\dagger \hat{H}_{\mathbf{k}\sigma}^{\text{MF}} \Psi_{\mathbf{k}\sigma}, \quad (27)$$

where the summation symbol with prime denotes the summation over the reduced Brillouin zone, and  $4 \times 4$  matrix  $\hat{H}_{\mathbf{k}\sigma}^{\text{MF}}$  equals to

$$\hat{H}_{\mathbf{k}\sigma}^{\text{MF}} = - \begin{pmatrix} \Delta_\sigma & tf(\mathbf{k}_\parallel) & t_0g(k_z) & 0 \\ tf^*(\mathbf{k}_\parallel) & -\Delta_\sigma & 0 & t_0g(k_z) \\ t_0g^*(k_z) & 0 & -\Delta_\sigma & tf(\mathbf{k}_\parallel) \\ 0 & t_0g^*(k_z) & tf^*(\mathbf{k}_\parallel) & \Delta_\sigma \end{pmatrix}. \quad (28)$$

Here,  $\Delta_\uparrow = \Delta$ , and  $\Delta_\downarrow = -\Delta$ , and function  $g$  is defined as  $g(k_z) = 1 + e^{2ik_z c}$ . Matrix  $\hat{H}_{\mathbf{k}\sigma}^{\text{MF}}$  can be easily diagonalized. The mean-field eigenenergies are independent of electron spin and equal to

$$E_{\mathbf{k}}^{(1)} = -\sqrt{\Delta^2 + [tf(\mathbf{k}_\parallel) + 2t_0 \cos(ck_z)]^2}, \quad (29)$$

$$E_{\mathbf{k}}^{(2)} = -\sqrt{\Delta^2 + [tf(\mathbf{k}_\parallel) - 2t_0 \cos(ck_z)]^2}, \quad (30)$$

$$E_{\mathbf{k}}^{(3)} = \sqrt{\Delta^2 + [tf(\mathbf{k}_\parallel) - 2t_0 \cos(ck_z)]^2}, \quad (31)$$

$$E_{\mathbf{k}}^{(4)} = \sqrt{\Delta^2 + [tf(\mathbf{k}_\parallel) + 2t_0 \cos(ck_z)]^2}. \quad (32)$$

At half-filling and zero temperature  $T = 0$ , the first two bands are filled, the last two are empty, and the system is an insulator with the gap equal to  $2\Delta$ . Consequently, the zero-temperature mean-field energy is

$$E_{\text{MF}} = 2\mathcal{N} \frac{\Delta^2}{U} + 2 \sum_{\mathbf{k}}' (E_{\mathbf{k}}^{(1)} + E_{\mathbf{k}}^{(2)}). \quad (33)$$

Self-consistent equation for the order parameter is obtained by minimization of  $E_{\text{MF}}$  with respect to  $\Delta$ . Taking into account that  $\sum_{\mathbf{k}}' [E_{\mathbf{k}}^{(1)} + E_{\mathbf{k}}^{(2)}] = \sum_{\mathbf{k}} E_{\mathbf{k}}^{(2)}$ , where the summation on the right-hand side is performed over the full AA-G Brillouin zone, we can write the self-consistency equation  $\partial E_{\text{MF}}/\partial \Delta = 0$  as

$$\frac{2}{U} = \int_{-\infty}^{\infty} d\varepsilon \frac{\rho(\varepsilon)}{\sqrt{\Delta^2 + \varepsilon^2}}. \quad (34)$$

In this equation, the AA-G density of states  $\rho(\varepsilon)$  is defined according to the formula

$$\rho(\varepsilon) = \int \frac{d^3\mathbf{k}}{v_{\text{BZ}}} \delta[t|f_{\mathbf{k}_\parallel}| + 2t_0 \cos(k_z c) - \varepsilon], \quad (35)$$

in which the integration is performed over the full AA-G Brillouin zone, and  $v_{\text{BZ}} = 16\pi^3/(3\sqrt{3}ca^2)$  is the Brillouin zone volume. Since for any  $\mathbf{k}_\parallel$  one has  $0 < |f(\mathbf{k}_\parallel)| < 3$ , the density of states (35) is nonzero in the range  $-2t_0 < \varepsilon < 3t + 2t_0$ .

It is convenient to express the density of states [Eq. (35)] as a sum

$$\rho(\varepsilon) = \rho_{\text{gr}}(\varepsilon)\Theta(\varepsilon) + \delta\rho(\varepsilon), \quad (36)$$

where  $\rho_{\text{gr}}(\varepsilon)$  is the density of states of the single-layer graphene,  $\Theta(\varepsilon)$  is the Heaviside step function, and correction  $\delta\rho(\varepsilon)$  vanishes when  $t_0 = 0$ . The term  $\delta\rho$  corresponds to modification of the density of states due to the interlayer hopping. In the (realistic) limit  $t_0 \ll t$  and for small energy  $\varepsilon \ll t$  the following approximate expression for  $\delta\rho$  may be established (see Appendix A):

$$\delta\rho(\varepsilon) \approx \frac{2}{\sqrt{3}\pi^2 t^2} \Theta(2t_0 - |\varepsilon|) \times \left[ \sqrt{4t_0^2 - \varepsilon^2} - |\varepsilon| \arccos\left(\frac{|\varepsilon|}{2t_0}\right) \right]. \quad (37)$$

Formally, this expression was derived in the low-energy limit  $\varepsilon \ll t$ . Fortunately, decomposition (36) with  $\delta\rho$  given by Eq. (37) works quite well almost everywhere, except near the van Hove singularity  $\varepsilon \sim t$ , and the band edge  $\varepsilon \sim 3t$  (see discussion in Appendix A and Fig. 4).

Equations (36) and (37) allow one to estimate the integral in Eq. (34) and obtain an analytical expression for the SDW order parameter in the limit  $\Delta \ll t$ . To this end, we rewrite Eq. (34) in the following manner:

$$\frac{2}{U} = \int_0^{3t} d\varepsilon \frac{\rho_{\text{gr}}(\varepsilon)}{\sqrt{\Delta^2 + \varepsilon^2}} + \int_{-2t_0}^{2t_0} d\varepsilon \frac{\delta\rho(\varepsilon)}{\sqrt{\Delta^2 + \varepsilon^2}}. \quad (38)$$

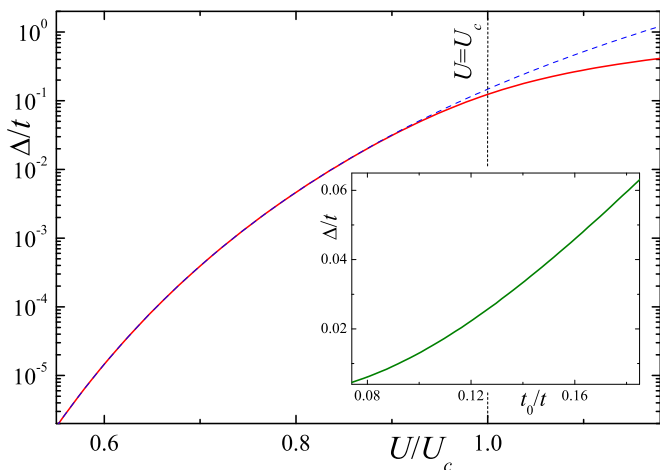


FIG. 3. The dependence of the SDW order parameter on the onsite repulsion energy  $U$ . The plots are calculated for  $t_0 = 0.37$  eV and  $t = 2.7$  eV, which corresponds to the ratio  $t_0/t = 0.136$ . Red solid curve is found numerically by solving Eq. (34), while dashed blue curve corresponds to approximate formula (42). Inset shows the dependence of  $\Delta$  on  $t_0$  calculated by solving Eq. (34) at  $U/U_c = 0.9$ .

Since  $\rho_{\text{gr}}(\varepsilon) \propto \varepsilon$  at small energies, the first integral in this formula is well defined for  $\Delta \rightarrow 0$ . It equals

$$\int_0^{3t} d\varepsilon \frac{\rho_{\text{gr}}(\varepsilon)}{\sqrt{\Delta^2 + \varepsilon^2}} \approx \int_0^{3t} d\varepsilon \frac{\rho_{\text{gr}}(\varepsilon)}{\varepsilon} \equiv \frac{2}{U_c}. \quad (39)$$

Constant  $U_c$ , defined by this equation, has the dimension of energy. Its physical meaning will be described below. Numerical calculations of the integral (39) with full density of states of graphene give  $U_c = 2.23t$ . For  $t = 2.7$  eV, we have  $U_c \approx 6.02$  eV.

The second integral in Eq. (38) diverges logarithmically when  $\Delta$  vanishes. It requires a more cautious approach. The detailed calculations are relegated to Appendix B. The resultant expression is

$$\int_{-2t_0}^{2t_0} d\varepsilon \frac{\delta\rho(\varepsilon)}{\sqrt{\Delta^2 + \varepsilon^2}} \approx 2\rho_0 \left( \ln \frac{8t_0}{\Delta} - 2 \right), \quad (40)$$

where the AA-G density of states at the Fermi level equals

$$\rho_0 = \rho(0) = \delta\rho(0) \approx \frac{4t_0}{\sqrt{3}\pi^2 t^2}. \quad (41)$$

Combining Eqs. (38), (39), and (40), we derive the following relation for the SDW order parameter:

$$\Delta \approx 8t_0 \exp \left[ -\frac{1}{\rho_0} \left( \frac{1}{U} - \frac{1}{U_c} \right) - 2 \right]. \quad (42)$$

This equation is valid for small  $\Delta$ . As the gap grows, this analytical expression becomes progressively less accurate. In such a situation, one is forced to solve Eq. (34) numerically. The dependence of  $\Delta$  on  $U$  calculated numerically and estimated according to approximation (42) are shown in Fig. 3. The data

in the figure demonstrate an excellent agreement between the two approaches if  $U < U_c$ .

## IV. DISCUSSION

### A. Single-layer graphene physics in SDW transition

Our theory implies that the AA-G is a SDW insulator at low temperature. The value of the insulating gap  $2\Delta$  substantially depends on the interaction parameter  $U$  and the interlayer hopping amplitude  $t_0$  [see inset to Fig. 3 and Eq. (42)]. The sensitivity to  $U$  is a familiar feature of a mean-field theory. As for the dependence on  $t_0$ , it is a consequence of the fact that the AA-G density of states at the Fermi level  $\rho_0$  is proportional to  $t_0$ . Reducing  $t_0$  to zero, we enter a regime where our model describes a collection of decoupled graphene layers. Due to its importance, let us analyze this limit in more detail.

Equation (42) implies that  $\Delta \rightarrow 0$  when  $t_0 \rightarrow 0$ , provided that  $U$  is smaller than the critical threshold  $U_c$ . For  $U > U_c$ , Eq. (42) predicts that  $\Delta$  diverges when  $t_0 \rightarrow 0$ , indicating the failure of approximation (42) for large  $U$ . The value  $U_c \approx 2.23t \approx 6.02$  eV is found using Eq. (39). It can be also calculated from Eq. (34) in the limit  $\Delta = t_0 = 0$ .

The difference between  $U < U_c$  and  $U > U_c$  regimes is physically significant. Once  $U > U_c$ , Eq. (34) has a solution even for uncoupled layers, when  $t_0 = 0$ . In other words, the ground state of the Hubbard model for single graphene layer is antiferromagnetic for  $U > U_c$ . This is a well-known result [20–22]. The experiments show that graphene remains semimetal even at low temperatures. Thus, we expect that  $U < U_c$ . The approach exploring Monte Carlo simulations [20,21] gives  $U_c/t \approx 4.5$  (or  $U_c \approx 12.15$  eV for  $t = 2.7$  eV), which is larger than the presented above mean-field result  $U_c \approx 2.23t \approx 6.02$  eV [22]. *Ab initio* calculations of the Hubbard  $U$  in graphene performed in Ref. [23] give  $U \approx 9.3$  eV, that is, the value close, but somewhat smaller than critical value  $U_c$  obtained by Monte Carlo simulations. While the single-layer graphene physics cannot generate the ordering transition for  $U < U_c$ , it affects the magnitude of  $\Delta$  significantly: large factor  $\exp[1/(\rho_0 U_c)]$  in Eq. (42) introduces strong renormalization of preexponential energy scale  $t_0$ .

### B. Comparison with AA bilayer graphene

The presented theory of the SDW order in AA graphite is an extension of SDW theory for the AA bilayer graphene, whose lattice has similar geometric structure. For the SDW order in AA bilayer graphene, the mean-field calculations have been reported in Refs. [17–19,24,25], the investigations by numerical methods have been presented in Refs. [26–29]. These results, as well as some others, were reviewed in Ref. [30].

Experimental data for AA graphene are quite limited. This is a consequence of small number of samples. If one is interested in possible SDW in AA bilayer graphene, there is additional experimental complication. The bilayer, being true 2D material, contains too little amount of matter for currently extant neutron scattering techniques to be of use. On the other hand, AA graphite is a 3D system. Therefore, synthesis of sufficiently bulky AA graphite samples may bear significant implications for understanding of possible magnetism of the AA bilayer graphene.

### C. Other types of order parameters

As it follows from Eqs. (21) and (22), the induced magnetization oscillates in space with the nesting wave vector  $\mathbf{Q}_0$ . This spatial modulation is an important feature for it guarantees the coupling of the two nested Fermi surface sheets, leading to the SDW instability. There are other order parameters, which oscillate in space with  $\mathbf{Q}_0$ . One of them was already mentioned above. It is the order parameter of the SDW type, with magnetization described by Eq. (21) in which  $S_\alpha$  is chosen according to  $S_A = S_B$ . This order corresponds to layered antiferromagnetic state. While it oscillates with the required wave vector  $\mathbf{Q}_0$ , it does not open a gap at Fermi level, and only modifies the Fermi surface. This can be easily shown performing calculations similar to that presented in the previous section. As a result, such an order cannot benefit from nesting. Similar argumentation was used in Ref. [17] for the AA bilayer graphene.

Another possible order parameter oscillating with wave vector  $\mathbf{Q}_0$  describes the CDW state. It can be written as

$$\Delta_{\mathbf{n}j\alpha}^{\text{CDW}} = \frac{U}{2} (\langle n_{\mathbf{n}j\alpha\uparrow} \rangle + \langle n_{\mathbf{n}j\alpha\downarrow} \rangle) = e^{i\mathbf{Q}_0 \cdot \mathbf{r}_{\mathbf{n}j}} \Delta_\alpha^{\text{CDW}}. \quad (43)$$

Similar to Eq. (24), the gap at Fermi level is opened, when  $\Delta_A^{\text{CDW}} = -\Delta_B^{\text{CDW}}$ . However, in our model, the CDW is stable only if  $U < 0$ , otherwise, such an order parameter is absolutely unstable. (In principle, even in repulsive models, the CDW can be induced by a sufficiently strong magnetic field [2,31,32], or lattice participation [33]. However, studying these factors is beyond the present discussion.)

### D. Denesting

It is important to discuss the effects of the violation of perfect nesting in our model. Analyzing Eq. (42), we notice that  $\Delta$  vanishes exponentially for vanishing interaction  $U$ , however, it remains finite for any finite  $U$ . In this respect, our calculations are very similar to the BCS result for superconducting order parameter. This feature is a consequence of the perfect nesting of the Fermi surface sheets. The perfect nesting is an approximation. It may be destroyed by longer-range hopping processes in the kinetic energy term. For a Fermi surface with an imperfect nesting, the interaction parameter  $U$  must exceed some critical strength  $U^*$  to induce the ordering transition [16]. The value of  $U^*$  depends on a degree of the denesting. Therefore, sufficiently strong denesting prevents SDW order by pushing  $U^*$  above  $U$ .

In addition to the longer-range hopping amplitudes, the denesting may be enhanced by doping: extra electrons “inflate” the electron Fermi surface sheet and “deflate” the hole sheet. The hole doping exerts the opposite effect on the sheets. Regardless of the sign of the doped charge, the shapes of the sheets become unequal after the doping, violating the nesting. Doping-induced denesting destabilizes the homogeneous state of the electron liquid. Theoretical studies of the inhomogeneous states (“stripes,” phase separation) were performed for a variety of systems [15,19,34–44]. It follows from this research that doped SDW systems have rich phase diagram and demonstrate interesting physical phenomena. Therefore, doped AA graphite might deserve a special investigation.

### E. Motivation for the use of the Hubbard Hamiltonian

It is well known that the use of the Hubbard model, with its extremely short-range interaction, may be partially justified in case of metals with short screening length. Unfortunately, the screening in AA graphite, as well as in graphene, bilayer graphene, and related materials is rather poor due to vanishing or low density of states at the Fermi energy.

For AA graphite, a possible alternative to the Hubbard interaction is the use of the screened Coulomb interaction consistent with small, but finite, number of the charge carriers. However, we believe that at the present phase of the research, the use of the Hubbard model is warranted. First of all, one must remember that the SDW instability in our model is nesting driven. Consequently, at the qualitative level, the SDW is fairly insensitive to details of the interaction. Furthermore, the mean-field calculations for the Hubbard Hamiltonian are simple and well understood. This ensures that mathematical details of the formalism will not obstruct the qualitative discussion. A more rigorous and complex analysis could be executed at later stages.

Currently, the Hubbard model is a common approach employed for description of graphene and related materials [45–49]. The ability of the Hubbard interaction to mimic properties of the longer-range interaction is also discussed [50]. Thus, it appears that, while not without its flaws, the Hubbard Hamiltonian is a suitable tool for the task at hand.

### F. Conclusions

In this paper, we have studied SDW order in AA graphite. Unlike the single-layer graphene, whose Fermi surface shrinks to two Fermi points, AA graphite has a well-developed two-sheet Fermi surface. This Fermi surface is a consequence of interlayer tunneling, and it disappears when the tunneling vanishes. The SDW instability is driven by the nesting of two Fermi surface sheets. Straightforward mean-field calculations allow one to estimate the SDW order-parameter magnitude. The derived expression for the SDW magnetization shows strong enhancement due to single-layer-graphene electron states.

### ACKNOWLEDGMENT

This work is partially supported by the Russian Foundation for Basic Research (Project No. 17-02-00323).

### APPENDIX A: CALCULATION OF DENSITY OF STATES

In this appendix, we calculate density of states  $\rho(\varepsilon)$ , which is defined by Eq. (35). In general, the argument of the  $\delta$  function in the integral of Eq. (35) is complicated. However, in the limit  $\varepsilon \ll t$  and  $t_0 \ll t$  one can replace  $t|f_{\mathbf{k}_\parallel}| \approx v_F|\mathbf{q}|$ . In this regime, we evaluate the integral in Eq. (35) explicitly:

$$\begin{aligned} \rho(\varepsilon) &= \int \frac{d^3\mathbf{k}}{v_{\text{BZ}}} \delta(t|f_{\mathbf{k}_\parallel}| + 2t_0 \cos(k_z c) - \varepsilon) \\ &\approx N_D \int \frac{d^2\mathbf{q} dk_z}{v_{\text{BZ}}} \delta(v_F|\mathbf{q}| + 2t_0 \cos(k_z c) - \varepsilon) \end{aligned}$$

$$\begin{aligned}
 &= \frac{4\pi}{v_{\text{BZ}} \int_0^{2\pi/c} dk_z} \int_0^\infty q dq \delta(v_{\text{F}}q + 2t_0 \cos(k_z c) - \varepsilon) \\
 &= \frac{4\pi}{c v_{\text{F}}^2 v_{\text{BZ}}} \int_0^{2\pi} d\gamma (\varepsilon - 2t_0 \cos \gamma) \Theta(\varepsilon - 2t_0 \cos \gamma).
 \end{aligned} \tag{A1}$$

Symbol  $N_{\text{D}} = 2$  denotes the number of nonequivalent Dirac points, and  $\Theta(x)$  is the Heaviside step function. Taking into account that  $v_{\text{F}} = 3ta/2$  and  $v_{\text{BZ}} = 16\pi^3/(3\sqrt{3}ca^2)$ , the density of states  $\rho(\varepsilon)$  can be expressed as

$$\rho(\varepsilon) = \frac{2t_0}{\sqrt{3}\pi^2 t^2} F(\varepsilon/2t_0), \tag{A2}$$

where dimensionless function  $F(\xi)$  is equal to

$$\begin{aligned}
 F(\xi) &= \int_0^{2\pi} d\gamma (\xi - \cos \gamma) \Theta(\xi - \cos \gamma) = 2\pi \xi \Theta(\xi) \\
 &+ (2\sqrt{1 - \xi^2} + 2\xi \arcsin \xi - \pi |\xi|) \Theta(1 - |\xi|).
 \end{aligned} \tag{A3}$$

Combining the latter equation with Eq. (A2), we determine

$$\begin{aligned}
 \rho(\varepsilon) &= \frac{2\varepsilon}{\sqrt{3}\pi^2 t^2} \Theta(\varepsilon) + \frac{2}{\sqrt{3}\pi^2 t^2} \Theta(2t_0 - |\varepsilon|) \\
 &\times \left[ \sqrt{4t_0^2 - \varepsilon^2} - |\varepsilon| \arccos\left(\frac{|\varepsilon|}{2t_0}\right) \right].
 \end{aligned} \tag{A4}$$

The first term in this equation corresponds to the well-known low-energy approximation for the density of states of the single-layer graphene:

$$\rho_{\text{gr}}(\varepsilon) \approx \frac{2|\varepsilon|}{\sqrt{3}\pi^2 t^2}. \tag{A5}$$

The second term, which is equal to  $\delta\rho(\varepsilon)$  from Eq. (37), is the correction due to the interlayer tunneling. This correction is of the order of  $t_0/t$ . It is nonzero only for  $|\varepsilon| < 2t_0$ .

When the condition  $\varepsilon \ll t$  is violated, Eq. (A4) is no longer valid, and more elaborate approach is necessary. Integrating over  $\mathbf{k}_{\parallel} = (k_x, k_y)$  in Eq. (35) one derives

$$\rho(\varepsilon) = \int_0^{2\pi} \frac{d\gamma}{2\pi} \rho_{\text{gr}}(\varepsilon - 2t_0 \cos \gamma) \Theta(\varepsilon - 2t_0 \cos \gamma). \tag{A6}$$

This integral can be evaluated numerically, using, for example, numerically exact graphene density of state  $\rho_{\text{gr}}(\varepsilon)$ . As a result, one accurately obtains the density of states for Hamiltonian (12). However, for our mean-field treatment, a less rigorous form of  $\rho(\varepsilon)$  is acceptable: we can employ decomposition (36) with  $\delta\rho$  given by the approximate expression (37). Figure 4 attests to the quality of this approximation. We see that both functions are virtually identical except the energies near the van Hove singularity  $\varepsilon = t$  and the high-energy band edge  $\varepsilon = 3t$ . Such a success may be explained as follows. Expanding Eq. (A6) in powers of  $t_0$ , one writes

$$\rho(\varepsilon) \approx \rho_{\text{gr}}(\varepsilon) + t_0^2 \rho_{\text{gr}}''(\varepsilon). \tag{A7}$$

This expression is valid away from the van Hove singularity and spectrum edges, where function  $\rho_{\text{gr}}(\varepsilon)\Theta(\varepsilon)$  does not have well-defined derivatives. In Eq. (A7) the correction of the order of  $t_0$  is zero. Neglecting small terms of the order of  $t_0^2$ , we

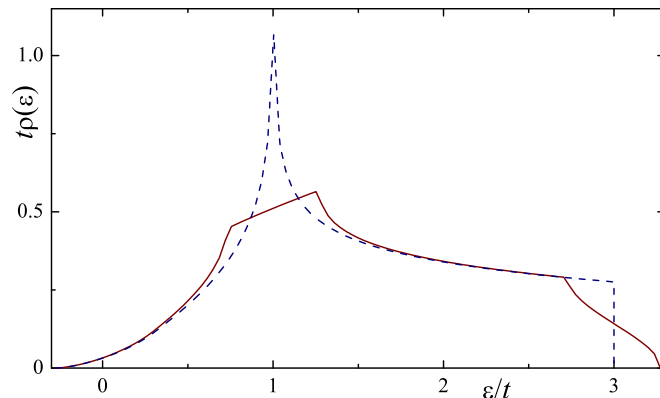


FIG. 4. The density of states of the AA graphite versus energy. The plots are calculated for  $t_0 = 0.37$  eV and  $t = 2.7$  eV, which corresponds to the ratio  $t_0/t = 0.136$ . Solid red curve is the result of numerical computation of integral in Eq. (35). Blue dashed curve corresponds to formula (36) in which approximate expression (37) for  $\delta\rho$  was used.

conclude that, away from the points  $\varepsilon = 0$ ,  $\varepsilon = t$ , and  $\varepsilon = 3t$ , we can approximate  $\rho(\varepsilon) \approx \rho_{\text{gr}}(\varepsilon)$ . Taking into account the low-energy correction  $\delta\rho(\varepsilon)$  [Eq. (37)], we capture the behavior of the density of states near  $\varepsilon = 0$ . Quality of approximation remains poor near  $\varepsilon = t$  and  $3t$ . These regions, fortunately, contribute weakly to the mean-field properties of the model. Thus, we accept that Eqs. (36) and (37) give a very good approximation to the AA-G density of states.

## APPENDIX B: EVALUATION OF THE SELF-CONSISTENCY EQUATION

In this appendix, we will evaluate the integral presented in Eq. (40). It diverges when  $\Delta \rightarrow 0$ . To evaluate this integral, the divergent term must be treated separately from the finite contribution. To this end, we write

$$\int_{-2t_0}^{2t_0} d\varepsilon \frac{\delta\rho(\varepsilon)}{\sqrt{\Delta^2 + \varepsilon^2}} = I_1 + I_2, \tag{B1}$$

where the quantities  $I_{1,2}$  are defined by the following relations:

$$I_1 = \int_{-2t_0}^{2t_0} d\varepsilon \frac{\delta\rho(\varepsilon) - \delta\rho(0)}{\sqrt{\Delta^2 + \varepsilon^2}}, \tag{B2}$$

$$I_2 = \int_{-2t_0}^{2t_0} d\varepsilon \frac{\delta\rho(0)}{\sqrt{\Delta^2 + \varepsilon^2}} = 2\rho_0 \operatorname{arsinh}\left(\frac{2t_0}{\Delta}\right). \tag{B3}$$

Symbol  $\rho_0$  is defined by Eq. (41). For small  $\Delta$  one has

$$I_2 \approx 2\rho_0 \ln\left(\frac{4t_0}{\Delta}\right). \tag{B4}$$

Integral  $I_1$  remains finite when  $\Delta \rightarrow 0$  and can be approximated by its value at  $\Delta = 0$ :

$$I_1 \approx \frac{8t_0}{\sqrt{3}\pi^2 t^2} \int_0^{2t_0} \frac{d\varepsilon}{\varepsilon} \left[ \sqrt{1 - \frac{\varepsilon^2}{4t_0^2}} - \frac{\varepsilon}{2t_0} \arccos\left(\frac{\varepsilon}{2t_0}\right) - 1 \right]. \tag{B5}$$

Since

$$\int_0^{2t_0} \frac{d\varepsilon}{2t_0} \arccos\left(\frac{\varepsilon}{2t_0}\right) = 1, \quad (\text{B6})$$

$$\int_0^{2t_0} \frac{d\varepsilon}{\varepsilon} \left[ \sqrt{1 - \frac{\varepsilon^2}{4t_0^2}} - 1 \right] = \ln 2 - 1, \quad (\text{B7})$$

we can estimate  $I_1$  as follows:

$$I_1 \approx \frac{8t_0}{\sqrt{3}\pi^2 t^2} (\ln 2 - 2) = 2\rho_0 (\ln 2 - 2). \quad (\text{B8})$$

Combining this expression with Eq. (B4), one obtains

$$\int_{-2t_0}^{2t_0} d\varepsilon \frac{\delta\rho(\varepsilon)}{\sqrt{\Delta^2 + \varepsilon^2}} \approx 2\rho_0 \left( \ln \frac{8t_0}{\Delta} - 2 \right). \quad (\text{B9})$$

This concludes the derivation of Eq. (40).

- 
- [1] K. S. Novoselov, A. K. Geim, S. V. Morozov, D. Jiang, Y. Zhang, S. V. Dubonos, I. V. Grigorieva, and A. A. Firsov, Electric field effect in atomically thin carbon films, *Science* **306**, 666 (2004).
- [2] F. Arnold, A. Isidori, E. Kampert, B. Yager, M. Eschrig, and J. Saunders, Charge Density Waves in Graphite: Towards the Magnetic Ultraquantum Limit, *Phys. Rev. Lett.* **119**, 136601 (2017).
- [3] T. E. Weller, M. Ellerby, S. S. Saxena, R. P. Smith, and N. T. Skipper, Superconductivity in the intercalated graphite compounds  $C_6Yb$  and  $C_6Ca$ , *Nat. Phys.* **1**, 39 (2005).
- [4] J.-C. Charlier, X. Gonze, and J.-P. Michenaud, First-principles study of the stacking effect on the electronic properties of graphite(s), *Carbon* **32**, 289 (1994).
- [5] J. Borysiuk, J. Soltys, and J. Piechota, Stacking sequence dependence of graphene layers on SiC (0001) - Experimental and theoretical investigation, *J. Appl. Phys.* **109**, 093523 (2011).
- [6] J.-K. Lee, S.-C. Lee, J.-P. Ahn, S.-C. Kim, J. I. B. Wilson, and P. John, The growth of AA graphite on (111) diamond, *J. Chem. Phys.* **129**, 234709 (2008).
- [7] Z. Liu, K. Suenaga, P. J. F. Harris, and S. Iijima, Open and Closed Edges of Graphene Layers, *Phys. Rev. Lett.* **102**, 015501 (2009).
- [8] H.-V. Roy, C. Kallinger, and K. Sattler, Study of single and multiple foldings of graphitic sheets, *Surf. Sci.* **407**, 1 (1998).
- [9] J.-C. Charlier, J.-P. Michenaud, X. Gonze, and J.-P. Vigneron, Tight-binding model for the electronic properties of simple hexagonal graphite, *Phys. Rev. B* **44**, 13237 (1991).
- [10] J.-C. Charlier, J.-P. Michenaud, and X. Gonze, First-principles study of the electronic properties of simple hexagonal graphite, *Phys. Rev. B* **46**, 4531 (1992).
- [11] A. Rozhkov, G. Giavaras, Y. P. Bliokh, V. Freilikher, and F. Nori, Electronic properties of mesoscopic graphene structures: Charge confinement and control of spin and charge transport, *Phys. Rep.* **503**, 77 (2011).
- [12] T. Rice, Band-structure effects in itinerant antiferromagnetism, *Phys. Rev. B* **2**, 3619 (1970).
- [13] E. Fawcett, Spin-density-wave antiferromagnetism in chromium, *Rev. Mod. Phys.* **60**, 209 (1988).
- [14] I. Eremin and A. V. Chubukov, Magnetic degeneracy and hidden metallicity of the spin-density-wave state in ferropnictides, *Phys. Rev. B* **81**, 024511 (2010).
- [15] L. P. Gor'kov and G. B. Teitel'baum, Spatial inhomogeneities in iron pnictide superconductors: The formation of charge stripes, *Phys. Rev. B* **82**, 020510 (2010).
- [16] A. O. Sboychakov, A. V. Rozhkov, K. I. Kugel, A. L. Rakhmanov, and F. Nori, Electronic phase separation in iron pnictides, *Phys. Rev. B* **88**, 195142 (2013).
- [17] A. L. Rakhmanov, A. V. Rozhkov, A. O. Sboychakov, and F. Nori, Instabilities of the AA-Stacked Graphene Bilayer, *Phys. Rev. Lett.* **109**, 206801 (2012).
- [18] A. O. Sboychakov, A. L. Rakhmanov, A. V. Rozhkov, and F. Nori, Metal-insulator transition and phase separation in doped AA-stacked graphene bilayer, *Phys. Rev. B* **87**, 121401 (2013).
- [19] A. O. Sboychakov, A. V. Rozhkov, A. L. Rakhmanov, and F. Nori, Antiferromagnetic states and phase separation in doped AA-stacked graphene bilayers, *Phys. Rev. B* **88**, 045409 (2013).
- [20] Z. Y. Meng, T. C. Lang, S. Wessel, F. F. Assaad, and A. Muramatsu, Quantum spin liquid emerging in two-dimensional correlated Dirac fermions, *Nature (London)* **464**, 847 (2010).
- [21] S. Sorella and E. Tosatti, Semi-Metal-Insulator Transition of the Hubbard Model in the Honeycomb Lattice, *Europhys. Lett.* **19**, 699 (1992).
- [22] N. M. R. Peres, M. A. N. Araújo, and D. Bozi, Phase diagram and magnetic collective excitations of the Hubbard model for graphene sheets and layers, *Phys. Rev. B* **70**, 195122 (2004).
- [23] T. O. Wehling, E. Şaşıoğlu, C. Friedrich, A. I. Lichtenstein, M. I. Katsnelson, and S. Blügel, Strength of Effective Coulomb Interactions in Graphene and Graphite, *Phys. Rev. Lett.* **106**, 236805 (2011).
- [24] R. S. Akzyanov, A. O. Sboychakov, A. V. Rozhkov, A. L. Rakhmanov, and F. Nori, AA-stacked bilayer graphene in an applied electric field: Tunable antiferromagnetism and coexisting exciton order parameter, *Phys. Rev. B* **90**, 155415 (2014).
- [25] L. Brey and H. A. Fertig, Gapped phase in AA-stacked bilayer graphene, *Phys. Rev. B* **87**, 115411 (2013).
- [26] D. S. de la Peña, M. M. Scherer, and C. Honerkamp, Electronic instabilities of the AA-honeycomb bilayer, *Ann. Phys. (Leipzig)* **526**, 366 (2014).
- [27] A. Nikolaev and M. Ulybyshev, PoS (LATTICE2014) 054.
- [28] A. Nikolaev and M. Ulybyshev, Monte-Carlo study of the phase transition in the AA-stacked bilayer graphene, [arXiv:1412.1359](https://arxiv.org/abs/1412.1359).



- [29] P. V. Buividovich and M. V. Ulybyshev, Applications of lattice QCD techniques for condensed matter systems, *Int. J. Mod. Phys. A* **31**, 1643008 (2016).
- [30] A. Rozhkov, A. Sboychakov, A. Rakhmanov, and F. Nori, Electronic properties of graphene-based bilayer systems, *Phys. Rep.* **648**, 1 (2016).
- [31] D. Yoshioka and H. Fukuyama, Electronic phase transition of graphite in a strong magnetic field, *J. Phys. Soc. Jpn.* **50**, 725 (1981).
- [32] D. Andres, M. V. Kartsovnik, W. Biberacher, H. Weiss, E. Balthes, H. Müller, and N. Kushch, Orbital effect of a magnetic field on the low-temperature state in the organic metal  $\alpha - (\text{BEDT} - \text{TTF})_2\text{KHg}(\text{SCN})_4$ , *Phys. Rev. B* **64**, 161104 (2001).
- [33] M. D. Johannes and I. I. Mazin, Fermi surface nesting and the origin of charge density waves in metals, *Phys. Rev. B* **77**, 165135 (2008).
- [34] J. Zaanen and O. Gunnarsson, Charged magnetic domain lines and the magnetism of high- $T_c$  oxides, *Phys. Rev. B* **40**, 7391 (1989).
- [35] A. Gorbatshevich, Y. Kopaev, and I. Tokatly, Band theory of phase stratification, *Zh. Eksp. Teor. Fiz.* **101**, 971 (1992) [*Sov. Phys.-JETP* **74**, 521 (1992)].
- [36] D. E. Sheehy and L. Radzihovsky, BEC-BCS crossover, phase transitions and phase separation in polarized resonantly-paired superfluids, *Ann. Phys.* **322**, 1790 (2007).
- [37] A. O. Sboychakov, K. I. Kugel, A. L. Rakhmanov, and D. I. Khomskii, Phase separation in doped systems with spin-state transitions, *Phys. Rev. B* **80**, 024423 (2009).
- [38] P. A. Igoshev, M. A. Timirgazin, A. A. Katanin, A. K. Arzhnikov, and V. Y. Irkhin, Incommensurate magnetic order and phase separation in the two-dimensional Hubbard model with nearest- and next-nearest-neighbor hopping, *Phys. Rev. B* **81**, 094407 (2010).
- [39] A. L. Rakhmanov, A. V. Rozhkov, A. O. Sboychakov, and F. Nori, Phase separation of hydrogen atoms adsorbed on graphene and the smoothness of the graphene-graphene interface, *Phys. Rev. B* **85**, 035408 (2012).
- [40] A. L. Rakhmanov, A. V. Rozhkov, A. O. Sboychakov, and F. Nori, Phase separation of antiferromagnetic ground states in systems with imperfect nesting, *Phys. Rev. B* **87**, 075128 (2013).
- [41] A. Bianconi, N. Poccia, A. Sboychakov, A. Rakhmanov, and K. Kugel, Intrinsic arrested nanoscale phase separation near a topological Lifshitz transition in strongly correlated two-band metals, *Supercond. Sci. Technol.* **28**, 024005 (2015).
- [42] A. O. Sboychakov, A. L. Rakhmanov, K. I. Kugel, A. V. Rozhkov, and F. Nori, Magnetic field effects in electron systems with imperfect nesting, *Phys. Rev. B* **95**, 014203 (2017).
- [43] A. V. Rozhkov, A. L. Rakhmanov, A. O. Sboychakov, K. I. Kugel, and F. Nori, Spin-Valley Half-Metal as a Prospective Material for Spin Valleytronics, *Phys. Rev. Lett.* **119**, 107601 (2017).
- [44] A. L. Rakhmanov, K. I. Kugel, M. Y. Kagan, A. V. Rozhkov, and A. Sboychakov, Inhomogeneous electron states in the systems with imperfect nesting, *JETP Lett.* **105**, 806 (2017).
- [45] J. Nilsson, A. H. Castro Neto, N. M. R. Peres, and F. Guinea, Electron-electron interactions and the phase diagram of a graphene bilayer, *Phys. Rev. B* **73**, 214418 (2006).
- [46] R. Dillenschneider and J. H. Han, Exciton formation in graphene bilayer, *Phys. Rev. B* **78**, 045401 (2008).
- [47] T. C. Lang, Z. Y. Meng, M. M. Scherer, S. Uebelacker, F. F. Assaad, A. Muramatsu, C. Honerkamp, and S. Wessel, Antiferromagnetism in the Hubbard Model on the Bernal-Stacked Honeycomb Bilayer, *Phys. Rev. Lett.* **109**, 126402 (2012).
- [48] J. Yuan, D.-H. Xu, H. Wang, Y. Zhou, J.-H. Gao, and F.-C. Zhang, Possible half-metallic phase in bilayer graphene: Calculations based on mean-field theory applied to a two-layer Hubbard model, *Phys. Rev. B* **88**, 201109 (2013).
- [49] J. Sun, D.-H. Xu, Y. Zhou, and F.-C. Zhang, Electrically controllable magnetic order in the bilayer Hubbard model on honeycomb lattice: A determinant quantum Monte Carlo study, *Phys. Rev. B* **90**, 125429 (2014).
- [50] M. Schüler, M. Rösner, T. O. Wehling, A. I. Lichtenstein, and M. I. Katsnelson, Optimal Hubbard Models for Materials with Nonlocal Coulomb Interactions: Graphene, Silicene, and Benzene, *Phys. Rev. Lett.* **111**, 036601 (2013).